Properties of phase transition of ice binding protein from Arctic yeast (LeIBP) utilizing differential scanning calorimetry (DSC) and Raman spectroscopy

Sanghwa Lee[a,b], Jun Hyuck Lee[c,d], Han-Woo Kim[c,d], Jong Wook Hong[b,e,*]

[a] Department of Bionano Engineering, Hanyang University, Kyunggi-do, 15588, Republic of Korea
[b] Biomedical Engineering Research Center, Asan Medical Center, University of Ulsan College of Medicine, Seoul, 05505, Republic of Korea
[c] Unit of Polar Genomics, Korea Polar Research Institute, Incheon, 21990, Republic of Korea
[d] Department of Polar Sciences, University of Science and Technology, Incheon, 21990, Republic of Korea
[e] Department of Bionano Technology, Graduate School, Hanyang University, Seoul, 04763, Republic of Korea

ABSTRACT

Ice binding proteins (IBPs) have been attracting significant interest on account of their characteristic of inhibiting ice growth and recrystallization. Owing to their unique characteristics, IBPs have been studied for applications in food, pharmaceuticals, and medicine, as well as from a general scientific point of view. In this study, we have used differential scanning calorimetry (DSC) and Raman spectroscopy as tools to understand the ice binding activity of the Arctic-yeast-originating extracellular ice binding glycoprotein (LeIBP) isolated from Leucosporidium sp. AY30. From the DSC results, an increase in the specific heat capacity was confirmed for 1 mg/mL LeIBP, which suggested that additional heat flow was required for the change in temperature. In addition, the temperature corresponding to the phase change of the solution was measured, and Raman spectroscopy was carried out on the frozen and molten phases, respectively. From the results of Raman analysis, we confirmed that the helical vibrations related to the ice binding sites on LeIBP were dramatically suppressed when the LeIBP solution was frozen. Furthermore, principal component analysis (PCA) of the Raman spectra yielded the contrast factor between the freezing and melting states. Both DSC and Raman spectroscopy are widely used to study the ice binding activity and the structural changes associated with molecular vibrations in cryobiology.

1. Introduction

Antifreeze proteins (AFP) and ice-binding proteins (IBP) have attracted much attention owing to their inhibitory effects on growth and recrystallization of ice, and their role in organism survival, including protection of stem cells and blood cells in cold environments. Even though chemically synthesized antifreezing agents, such as glycerol and dimethyl sulfoxide (DMSO), have been frequently used as cryoprotective agents (CPAs), they are associated with low cell viability [5]. To prevent chemical and cryogenic toxicity, AFP and IBP have been extracted from natural organisms, such as fish [2,6], plants [8,9,27], bacteria [13,14,24,25], and insects [3,4,7,15]. Furthermore, some microorganisms that live in cold environments can be grown at subzero (Celsius) temperatures because they are able to synthesize cold-adapted enzymes. Accordingly, an extracellular ice-binding glycoprotein (LeIBP) was isolated from Arctic yeast *Leucosporidium* sp. AY30 [17,23]. When LeIBP was introduced for cryopreservation of red blood cells, the

rate of hemolysis was reduced and the blood cell recovery rate was enhanced four-fold [18]. LeIBP activity has been characterized by employing thermal hysteresis (TH) and ice recrystallization inhibition (IRI) to investigate differences between freezing and thawing, and inhibition of the growth of large grains of ice that are damaging to cells, respectively [23]. However, confirming production and antifreeze activity is time-consuming because acquisition of molecular information and notification of whether IBP are bound on an ice surface require long and sensitive crystallization pretreatment procedures.

Raman spectroscopy has been studied for the verification of various biological samples, such as tissue [11,12], cells [1,28,30], bacteria [20,31], and proteins [21,22,26]. Raman spectroscopy is based on inelastic scattering of photons incident on the sample. When photons irradiate the sample, the initial photon energy is transferred to the sample by molecular vibrations. Because the initial single energy level of the photons is differentiated by various molecular vibration modes, the individual peaks of the obtained spectrum indicate the molecular

---

composition. Therefore, Raman measurements are an excellent tool for identifying biomaterials. Previous reports of other groups have shown that characterization of protein structure was consistent with circular dichroism studies [22] and reviewed protein changes detected by Raman spectroscopy in secondary protein structure [10,22,26]. Raman spectroscopy for the examination of antifreeze and ice-binding activity has the advantages of being continuous, nondestructive, and able to monitor molecular vibrations.

In this work, DSC studies were carried out to determine the phase transition temperatures and heat flow properties of LeIBP. From the thermodynamic study, appropriate temperatures for Raman spectroscopy measurements were determined. Heat flow associated with exothermic and endothermic processes was analyzed to investigate phase transitions. Raman spectroscopy was performed on powder, solution, and cryo-states of LeIBP to acquire fingerprint signals associated with the three different states.

2. Materials and methods

2.1. Sample preparation of LeIBP

Ice binding protein from Arctic yeast (LeIBP) was expressed in *Pichia pastoris* and purified as described previously [19,23]. Briefly, the codon optimized LeIBP coding gene was synthesized (Bioneer, Daejeon, Korea) and cloned into a yeast pPICZαA expression vector (Invitrogen, USA) with *Xho*I and *Not*I restriction sites. The positive LeIBP expressing colony was selected and used for large scale protein expression. The transformant cells were grown in 3 l of YPD medium at 30 °C for 5 days. The cells were induced by daily 5 mL methanol addition. The expressed LeIBP was secreted into culture media after induction and the supernatant was harvested by removing cells with centrifugation at 3000 × g for 20 min at 4 °C. Then, it was transferred to an ion exchange (QFF) column and bound LeIBP was eluted with 50 mM Tris-HCl buffer, pH 8.0, containing 400 mM NaCl. The elution fractions were analyzed by SDS-PAGE and collected fractions containing LeIBP were further purified using a Superdex 200 size exclusion column (Amersham Pharmacia). The column was equilibrated with 50 mM Tris-HCl buffer, pH 8.0, containing 150 mM NaCl and sample was separated at a flow rate of 1 mL/min with same buffer. The finally purified LeIBP was then freeze-dried overnight (Labconco 79340-10 freeze dry system).

2.2. Differential scanning calorimetry (DSC) measurement

DSC (Q20 calorimeter, TA Instruments) was performed on LeIBP dissolved in water. Tzero low-mass pans with hermetic lids were filled with 5 μL of LeIBP solution, using a pipette (Eppendorf, Germany), and the temperature scanning range was −80 to 80 °C so that LeIBP is not denatured during the pretest. The temperature was decreased from 5 °C to the starting temperature of −80 °C, then increased to 80 °C, and finally decreased to −80 °C. After confirming that the exothermic peaks that occurred during the two cooling cycles overlapped, it was verified that there was no denaturing. With empty pans on the sample and reference stages, baseline correction was executed twice. The rate of temperature decrease was varied from 20 to 2 °C/min. The value of the exothermic peak was reproducible before it reached 10 °C/min, and hence, this rate was selected for the other samples.

2.3. Raman spectroscopy

Raman spectra were collected using a Horiba LabRam Aramis spectrometer with a diode laser (785 nm) as the excitation source. The light scattered inelastically by the sample was collected in a backscattering geometry using ×10 and ×50 microscope objective lens. The excitation beam spot sizes through the ×10 and ×50 objective lens were about 3.6 and 2 μm in diameter, respectively. The 1 mW power of the laser was attenuated using a power filter to obtain a good signal-to-

noise ratio (SNR) while avoiding the protein folding–unfolding process. To amplify the Raman signal using local surface plasmon resonance (LSPR), the LeIBP solution was dropped on gold nanoparticle (NP)-coated paper. Gold NPs were directly synthesized using gold chloride ($HAuCl_4$, > 99.9%) and sodium borohydride ($NaBH_4$, > 96%), and enriched by centrifugation at 3000 rpm for 1 h. The enriched gold NPs were dropped on Whatman cellulose chromatography paper (grade 1) and dried. All solutions of LeIBP and other reagents were prepared using 18.2 MΩ·cm distilled water. The samples were loaded on a temperature-controlled Linkam THMS600 stage mounted on a Raman sample stage. To evaluate the spectral differences between freezing and thawing of LeIBP solution, principal component analysis (PCA) was introduced. PCA is a statistical analysis method that reduces the number of variables in multivariate systems and Raman spectra have many peaks as variables. All analyses were conducted using XLSTAT 2016 software (see Fig. 1).

3. Results and discussion

3.1. Endothermic and exothermic behavior of LeIBP

DSC shows relative difference between the heat flow for LeIBP in water and the empty holder as a reference. During the cooling process at a constant rate of temperature decrease of 10 °C/min, heat is extracted from the solution. Because heat capacity is given by $\frac{Q}{\Delta T}$, where Q and T are heat and temperature, respectively, a heat flow greater than zero does not indicate an exothermic process, but the difference in the heat capacities of the target and reference samples, unless a specific peak is observed, as shown in Fig. 2 a (blue line). In the case of 1 mg/mL LeIBP solution, during cooling an increase was observed to −12.7 °C, followed by the rapid growth of a peak started at −22.7 °C. This was expected to contribute partially to the rise in the temperature of the sample itself before the heat generated from the exothermic event was transferred to the calorimeter. On the other hand, during the thawing process (Fig. 2 a, red line) a broader exothermic peak was observed. DSC measurements at various concentrations of LeIBP in water revealed a few intrinsic properties of the solutions in terms of heat capacity, melting, and thawing temperature, as shown in Fig. 2 b and 3.

During the cooling process, a phase transition from liquid to solid occurs, which is associated with an exothermic step in the heat capacity. Fig. 2 b shows the freezing behavior for various concentrations of LeIBP solution. The starting point of the exothermic peak is defined as the freezing point, which was −22.7, −17.1, −13.4, and −8.5 °C for the samples corresponding to 1, 0.1, 0.01, and 0.001 mg/mL, respectively. When the concentration of the solution in the iced state was changed from 0.001 to 1 mg/mL, the specific heat capacity varied from 0.498 to 0.642 cal/g·K. On the other hand, it changed from 1.002 to 1.224 cal/g·K for the liquid state. In the case of pure water, the specific heat capacities are 0.498 (solid) and 1.002 (liquid) Cal/g·K. On the other hand, the specific heat capacity of LeIBP powder only was ∼ 0.65 Cal/g·K at the freezing point. By considering the molar ratio between LeIBP and water in the case of the 1 mg/mL LeIBP solution, the solution has a higher heat capacity than the summation of the individual values for the powder and water. This observation indicated that LeIBP melted in water has intrinsic properties that are not the same as those of the powder, and it was expected that Raman spectra should reflect these differences. Unlike the freezing points, which varied with concentration, the variation of the melting points was very small at less than 1 °C. However, solutions with higher densities began to melt slightly below 0 °C, as shown Fig. 3. The maximum of the endothermic peak gradually moved to higher temperatures as the concentration of LeIBP decreased. When single Gaussian fitting was applied to the 1 mg/mL and water data, the peaks were centered at 3.5 and 4.7 °C, respectively. At the intermediate concentration of 0.01 mg/mL, the endothermic behavior appeared to be a two-step process corresponding to a summation of the 1 mg/mL solution and water results, as shown in
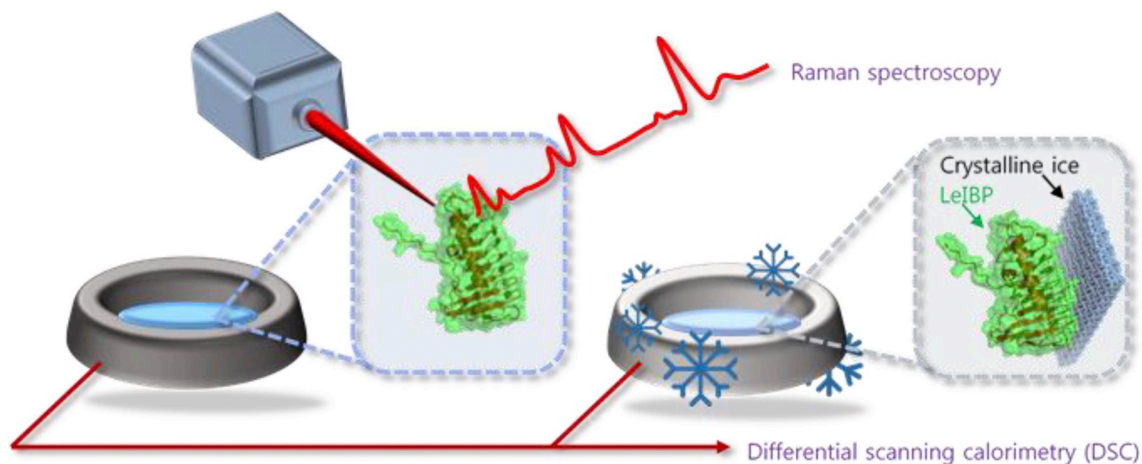
Fig. 1. Schematic diagram showing how phase transition of ice binding protein solution was examined using differential scanning calorimetry (DSC) and Raman spectroscopy.
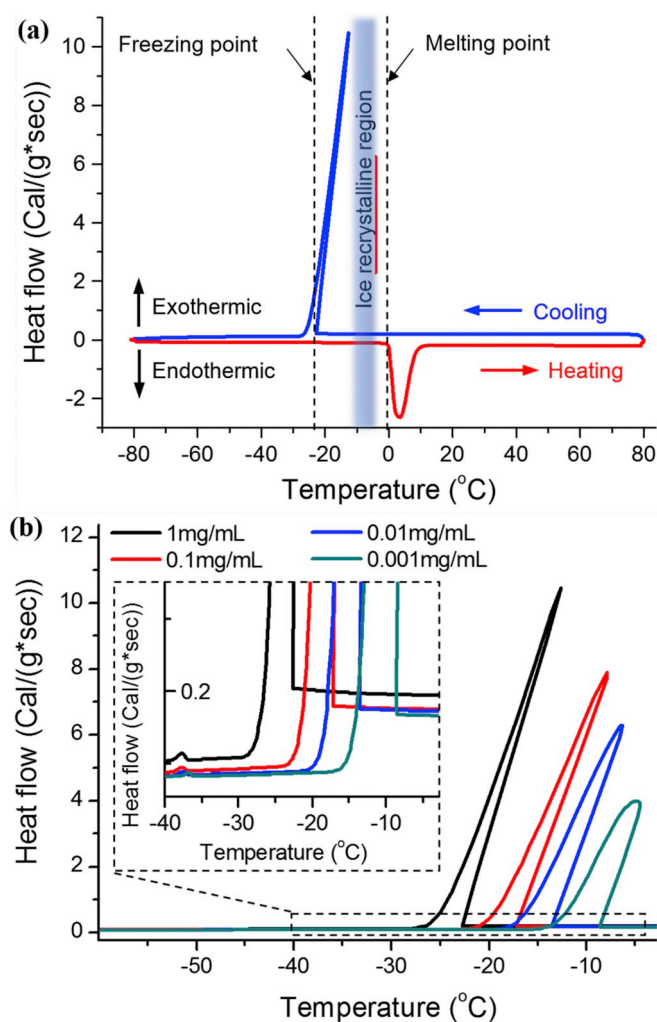

Fig. 2. (a) DSC curve of 1 mg/mL LeIBP in water. (b) Exothermic behavior of LeIBP in water (0.001–1 mg/mL). The area in the red dotted line is magnified in the inset, which shows a change heat capacity that indicates a phase transition after a rapid exothermic reaction. The peaks are slanted to the right because the Q20 calorimeter is a heat flux DSC that plots sample temperature instead of program temperature, and the temperature of the supercooled sample increases during freezing. (For interpretation of the references to colour in this figure legend, the reader is referred to the Web version of this article.)
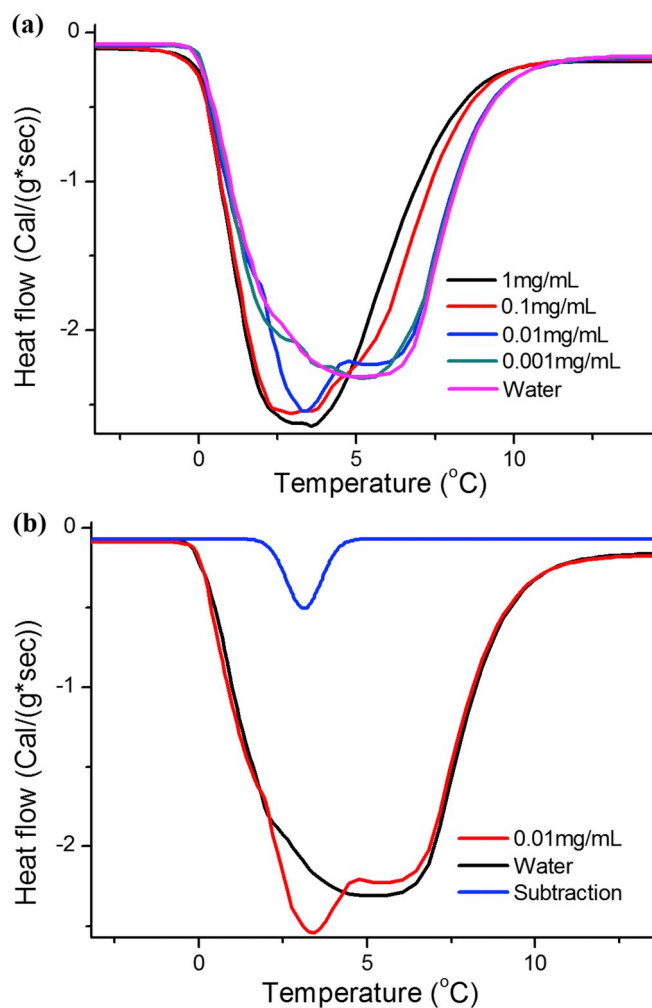

Fig. 3. Endothermic behavior of LeIBP with increasing temperature (a) at various concentrations from 0 (only water) to 1 mg/mL. (b) Peak center of Gaussian for subtraction between 0.01 mg/mL and water was located at 3.1 °C.

Fig. 3 b. Gaussian fitting of the data obtained by subtraction of the water results from the 0.01 mg/mL solution results revealed a peak centered at 3.1 °C. Thus, as an intrinsic characteristic for low concentrations of LeIBP in solution, it is estimated that the activity of LeIBP is localized during melting.
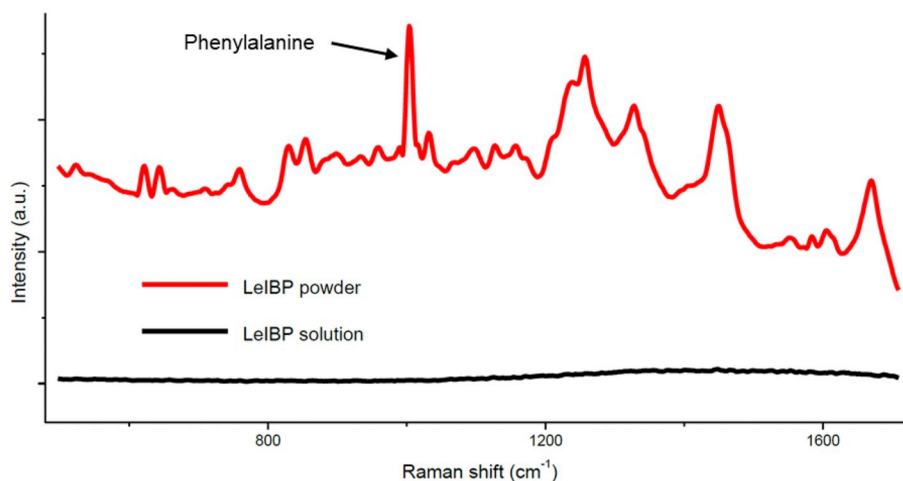
Fig. 4. Raman spectra of LeIBP solution and powder.

3.2. Raman measurement of LeIBP powder

The DSC results indicated the appropriate temperatures for Raman spectroscopy measurements because the observed changes in heat capacity correspond to phase transitions. As the temperatures between the exothermic and endothermic points are characterized by mixtures of liquid, solid, and crystalline ice states, the target temperatures for measuring Raman spectra were chosen as 15 and $-30\,°C$. These temperatures correspond to a stable temperature region of each phase, as obtained from the DSC results. Prior to investigating the phase transition of LeIBP solution, the differences between Raman spectra in solution and in the powder state were examined, as shown in Fig. 4. Even though solution did not show strong spectral peaks, the spectrum of dried LeIBP was the same as that of the initially extracted powder. Significant peaks located at 1002, 1256, 1327, 1449, and $1670\,cm^{-1}$ are related to phenylalanine, α-helix, and aliphatic amino acid components [29]. The very intense peak at around $1000\,cm^{-1}$ corresponds to phenylalanine, which is not sensitive to conformational changes in most of proteins. The peaks at 1256 and $1670\,cm^{-1}$ originate from the α-helix of the protein, which is a well-known spiral form. The peaks at 1327 and $1449\,cm^{-1}$ correspond to aliphatic amino acids, which have hydrophobic properties. These characteristic peaks have been described in a previous report on LeIBP structures [19]. From this peak assignment, the individual peaks in the Raman spectrum of LeIBP are sufficient for identifying isolated ice-binding proteins.

3.3. Surface enhanced Raman and statistical analysis of LeIBP solution

To investigate the solution state of LeIBP using Raman spectroscopy, paper coated with gold NPs was introduced as a surface enhanced Raman spectroscopy (SERS) substrate, which has the advantage of porosity. After dropping the $1\,mg/mL$ LeIBP solution on the SERS substrate, several Raman scans were acquired and averaged, as shown in Fig. 5. Each data point was obtained by varying the local position. The sample was allowed to stabilize for 5 min after changing the temperature. The main peaks for the LeIBP solution were observed at 950, 1000, 1100, 1170, 1265, 1320, and $1450\,cm^{-1}$, which corresponded to α-helices, phenylalanine, deformation vibrations of CH_x [16], and a paper-oriented peak. The phenylalanine peak at around $1000\,cm^{-1}$ increased dramatically when the liquid on the substrate dried (data not shown). This change is similar to that of the peak observed in the powder spectrum, shown in Fig. 4. Thus, it can be concluded that the Raman signal obtained at $-30\,°C$ (Fig. 5) is a result of the ice binding activity and indicates little effect of dehydration. The peak at $1100\,cm^{-1}$ corresponds not only to proline, alanine, and stretching vibrations of $C-C$ bonds, but is also a main peak of the paper used as

the SERS substrate. The spectra of pristine gold NP-coated paper and the protein on gold-coated glass confirmed that this peak has contributions from both the protein and paper.

The standard deviations of the peaks at 950, 1265, and $1450\,cm^{-1}$ in the spectra measured at $15\,°C$ (red line, Fig. 5) were significantly decreased when the temperature was $-30\,°C$ (blue line, Fig. 5). Note that these peaks correspond to the α-helix structure and are marked by black circles in Fig. 5. Previous structural results for LeIBP [11] revealed that β-helices provide ice-binding sites with a long α-helix packing structured exists along one face. The α-helix has the role of providing stabilization of the LeIBP components. This observation indicates why deviations of the helical vibrational peaks were inhibited for the frozen solution. First, the SERS substrate with gold NPs, which have small radii on the nanometer scale, acts as a Raman signal enhancer. Owing to the flexibility of the protein dissolved in water, LeIBP moves, rotates, and folds during irradiation by the excitation laser. Furthermore, absorption and desorption of LeIBP on the gold surface occurred frequently in the solution state. Second, specific peak intensities in the Raman spectra decreased owing to deformation by protein folding and increased owing to proximity to the gold surface. On the other hand, close proximity between LeIBP and the gold surface restricts rotation, movement, and protein folding in the frozen state. By occupying the β-helix binding site for crystalline ice, the α-helix was stabilized and became ordered, resulting in a significant reduction of the deviation in intensity related to the α-helix.

In addition to this deviation, PCA provided further discrimination between freezing and thawing of LeIBP solutions, as shown in Fig. 6. The first principle component explained 44.1% of the data and the fifth component explained 6.35%, with the ice and solution phase clustered near each other, divided by a dashed line. By using the variation in 1024 points between 500 and $1700\,cm^{-1}$ as a reference, it could be determined whether a sample is frozen.

4. Conclusion

In summary, the IBP isolated from the Arctic yeast *Leucosporidium* sp. AY30 (LeIBP) was characterized using DSC and Raman spectroscopy. The temperatures of the phase transitions of LeIBP solutions were acquired from the DSC results. The heat flow and thermal capacity results showed that dissolving LeIBP changed the properties of water. With reference to the DSC results, Raman measurements were performed at 15 and $-30\,°C$ to ensure that freezing and thawing were completely finished. Standard deviations of the Raman peaks corresponding to helical vibration modes were dramatically suppressed for the frozen LeIBP solution. It is estimated that the α-helix provides stabilization for the ice-binding site and the flexibility of the protein is reduced in the frozen state. By utilizing
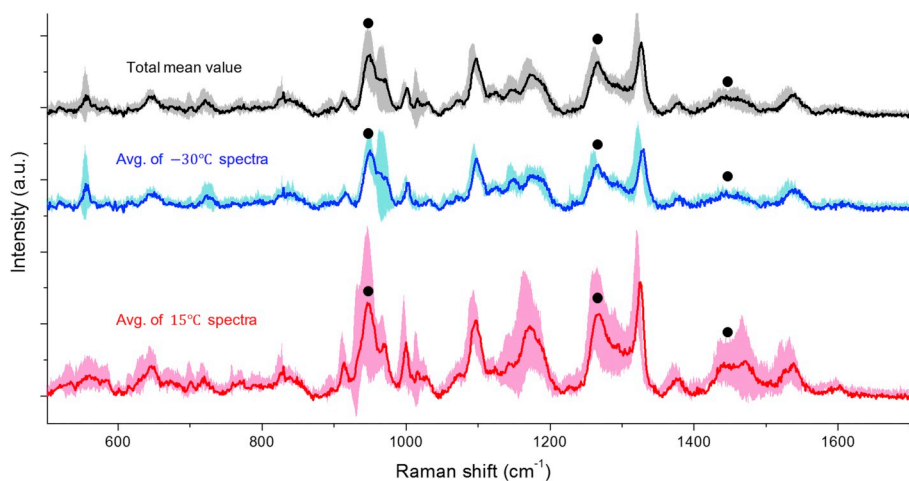
Fig. 5. Averaged Raman spectra for all samples (black line), and for freezing (blue line) and thawing (red line) of LeIBP solutions. Standard deviations are painted around the spectra. The peaks marked by black circles are due to helical vibrations. (For interpretation of the references to colour in this figure legend, the reader is referred to the Web version of this article.)
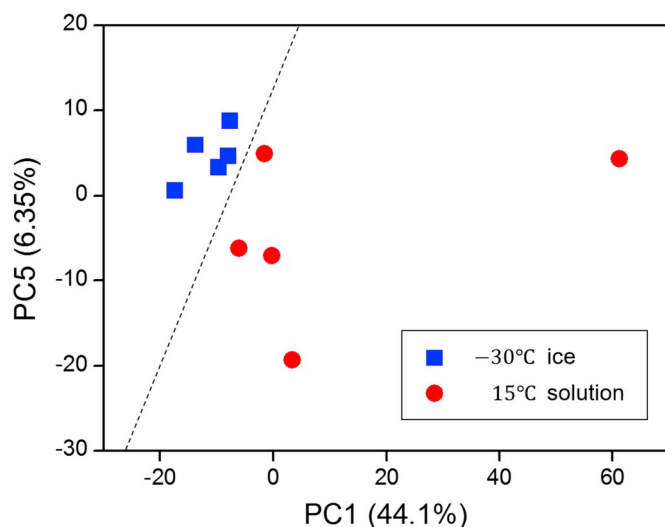

Fig. 6. Principle component analysis results for freezing and thawing of LeIBP solutions.

PCA tools, data corresponding to the frozen and thawed states were grouped successfully. From these results, we have confirmed that Raman analysis can bring useful information for identifying LeIBP and monitoring its ice-binding activities.

Conflicts of interest

The authors declare that they have no conflict of interest.

Appendix A. Supplementary data

Supplementary data to this article can be found online at https://doi.org/10.1016/j.cryobiol.2018.10.005.

References

[1] L.F. Carvalho, F. Bonnier, K. O'Callaghan, J. O'Sullivan, S. Flint, H.J. Byrne, F.M. Lyng, Raman micro-spectroscopy for rapid screening of oral squamous cell carcinoma, Exp. Mol. Pathol. 98 (2015) 502–509.

[2] R.W.R. Crevel, J.K. Fedyk, M.J. Spurgeon, Antifreeze proteins: characteristics, occurrence and human exposure, Food Chem. Toxicol. 40 (2002) 899–903.

[3] D. Doucet, M.G. Tyshenko, P.L. Davies, V.K. Walker, A family of expressed antifreeze protein genes from the moth, Choristoneura fumiferana, Eur. J. Biochem. 269 (2002) 38–46.

[4] J.G. Duman, V. Bennett, T. Sformo, R. Hochstrasser, B.M. Barnes, Antifreeze proteins in Alaskan insects and spiders, J. Insect Physiol. 50 (2004) 259–266.

[5] G.M. Fahy, The relevance of cryoprotectant toxicity to cryobiology, Cryobiology 23 (1986) 1–13.

[6] G.L. Fletcher, C.L. Hew, P.L. Davies, Antifreeze proteins of teleost fishes, Annu. Rev. Physiol. 63 (2001) 359–390.

[7] L.A. Graham, P.L. Davies, Glycine-rich antifreeze proteins from snow fleas, Science 310 (2005) 461-461.

[8] M. Griffith, M.W.F. Yaish, Antifreeze proteins in overwintering plants: a tale of two activities, Trends Plant Sci. 9 (2004) 399–405.

[9] M. Griffith, P. Ala, D.S.C. Yang, W.C. Hon, B.A. Moffatt, Antifreeze protein produced endogenously in winter rye leaves, Plant Physiol. 100 (1992) 593–596.

[10] A.M. Herrero, Raman spectroscopy for monitoring protein structure in muscle food systems, Crit. Rev. Food Sci. Nutr. 48 (2008) 512–523.

[11] M. Ishigaki, Y. Maeda, A. Taketani, B.B. Andriana, R. Ishihara, K. Wongravee, Y. Ozaki, H. Sato, Diagnosis of early-stage esophageal cancer by Raman spectroscopy and chemometric techniques, Analyst 141 (2016) 1027–1033.

[12] T. Kawabata, H. Kikuchi, S. Okazaki, M. Yamamoto, Y. Hiramatsu, J. Yang, M. Baba, M. Ohta, K. Kamiya, T. Tanaka, H. Konno, Near-infrared multichannel Raman spectroscopy with a 1064 nm excitation wavelength for ex vivo diagnosis of gastric cancer, J. Surg. Res. 169 (2011) e137–143.

[13] H. Kawahara, Y. Iwanaka, S. Higa, N. Muryoi, M. Sato, M. Honda, H. Omura, H. Obata, A novel, intracellular antifreeze protein in an Antarctic bacterium, Flavobacterium xanthum, Cryo Lett. 28 (2007) 39–49.

[14] H. Kawahara, Y. Nakano, K. Omiya, N. Muryoi, J. Nishikawa, H. Obata, Production of two types of ice crystal-controlling proteins in Antarctic bacterium, J. Biosci. Bioeng. 98 (2004) 220–223.

[15] E. Kristiansen, C. Wilkens, B. Vincents, D. Friis, A.B. Lorentzen, H. Jenssen, A. Lobner-Olesen, H. Ramlov, Hyperactive antifreeze proteins from longhorn beetles: some structural insights, J. Insect Physiol. 58 (2012) 1502–1510.

[16] J. Laane, Frontiers of Molecular Spectroscopy, first ed., Elsevier, Amsterdam ; Boston, 2009.

[17] J.H. Lee, A.K. Park, H. Do, K.S. Park, S.H. Moh, Y.M. Chi, H.J. Kim, Structural basis for antifreeze activity of ice-binding protein from arctic yeast, J. Biol. Chem. 287 (2012) 11460–11468.

[18] J.K. Lee, K.S. Park, S. Park, H. Park, Y.H. Song, S.H. Kang, H.J. Kim, An extracellular ice-binding glycoprotein from an Arctic psychrophilic yeast, Cryobiology 60 (2010) 222–228.

[19] S.G. Lee, H.Y. Koh, J.H. Lee, S.H. Kang, H.J. Kim, Cryopreservative effects of the recombinant ice-binding protein from the arctic yeast Leucosporidium sp. on red blood cells, Appl. Biochem. Biotechnol. 167 (2012) 824–834.

[20] T.Y. Liu, K.T. Tsai, H.H. Wang, Y. Chen, Y.H. Chen, Y.C. Chao, H.H. Chang, C.H. Lin, J.K. Wang, Y.L. Wang, Functionalized arrays of Raman-enhancing nanoparticles for capture and culture-free analysis of bacteria in human blood, Nat. Commun. 2 (2011) 538.

[21] F.M. Lyng, E.O. Faolain, J. Conroy, A.D. Meade, P. Knief, B. Duffy, M.B. Hunter, J.M. Byrne, P. Kelehan, H.J. Byrne, Vibrational spectroscopy for cervical cancer pathology, from biochemical analysis to diagnostic tool, Exp. Mol. Pathol. 82 (2007) 121–129.

[22] N.C. Maiti, M.M. Apetri, M.G. Zagorski, P.R. Carey, V.E. Anderson, Raman spectroscopic characterization of secondary structure in natively unfolded proteins:

alpha-synuclein, J. Am. Chem. Soc. 126 (2004) 2399–2408.

[23] K.S. Park, H. Do, J.H. Lee, S.I. Park, E. Kim, S.J. Kim, S.H. Kang, H.J. Kim, Characterization of the ice-binding protein from Arctic yeast Leucosporidium sp. AY30, Cryobiology 64 (2012) 286–296.

[24] J.A. Raymond, B.C. Christner, S.C. Schuster, A bacterial ice-binding protein from the Vostok ice core, Extremophiles 12 (2008) 713–717.

[25] J.A. Raymond, C. Fritsen, K. Shen, An ice-binding protein from an Antarctic sea ice bacterium, FEMS Microbiol. Ecol. 61 (2007) 214–221.

[26] A. Rygula, K. Majzner, K.M. Marzec, A. Kaczor, M. Pilarczyk, M. Baranska, Raman spectroscopy of proteins: a review, J. Raman Spectrosc. 44 (2013) 1061–1076.

[27] M. Smallwood, D. Worrall, L. Byass, L. Elias, D. Ashford, C.J. Doucet, C. Holt, J. Telford, P. Lillford, D.J. Bowles, Isolation and characterization of a novel

antifreeze protein from carrot (Daucus carota), Biochem. J. 340 (1999) 385–391.

[28] R. Smith, K.L. Wright, L. Ashton, Raman spectroscopy: an evolving technique for live cell studies, Analyst 141 (2016) 3590–3600.

[29] A. Synytsya, M. Judexova, D. Hoskovec, M. Miskovicova, L. Petruzelka, Raman spectroscopy at different excitation wavelengths (1064, 785 and 532 nm) as a tool for diagnosis of colon cancer, J. Raman Spectrosc. 45 (2014) 903–911.

[30] A.C.S. Talari, C.A. Evans, I. Holen, R.E. Coleman, I.U. Rehman, Raman spectroscopic analysis differentiates between breast cancer cell lines, J. Raman Spectrosc. 46 (2015) 421–427.

[31] H. Zhou, D. Yang, N.P. Ivleva, N.E. Mircescu, R. Niessner, C. Haisch, SERS detection of bacteria in water by in situ coating with Ag nanoparticles, Anal. Chem. 86 (2014) 1525–1533.